Numerical Analysis of Near-Infrared Wave Propagation Characteristics in Dielectric-Coated Parallel Planar Microstructural Waveguides

Wim E. A. Van Petegem, C. Robert James, Fred E. Vermeulen, *Member, IEEE* and Alexander M. Robinson

***Abstract*—In this paper, the properties of electromagnetic (EM) wave propagation in layered planar microstructural waveguides are investigated. Analytical and numerical results are presented on the propagation of a 1-μm EM wave in a parallel planar waveguide. Its walls are made of Au or Si, coated with a thin layer of SiO_2 and separated by a fluid. The propagation characteristics of even and odd TE and TM modes are described as a function of the coating thickness. It is shown that the propagation of TE modes exhibits a sudden shift in power flow distribution from the fluid to the coating when the coating thickness exceeds a critical value. This property may be exploited for micromachined sensor applications. TM modes do not exhibit this behavior.**

***Index Terms*—Coplanar waveguides, microsensor, submillimeter wave propagation.**

I. Introduction

THE PRESENT study examines the propagation properties in layered planar microstructural waveguides. Such structures have potential applications for micromachined sensor systems.

In earlier work [1], the authors have presented analytical and numerical results on the propagation characteristics of TE and TM modes in empty parallel-plane microstructural waveguides made of gold for wavelengths of 1–10 μm. Similar studies have been reported by the authors as well as others for cylindrical waveguides of gold and nickel [2]–[4]. Recently, changes of mode structures and attenuations in dielectric-coated circular hollow waveguides have been described in [5].

In this paper, the work in [1] and [5] is now extended to the analysis of 1-μm wave propagation in a symmetric parallel five-layer planar waveguide. Included in this study is the case where the metal constituting the conducting wall is gold, as in previous work [1]. However, silicon as wall material is also studied, for two reasons: 1) silicon is readily coated with SiO_2, since a native layer of SiO_2 normally exists on its surface; and 2) silicon has optical characteristics that greatly differ from those of gold: at 1-μm wavelength the refractive index of silicon is much higher than that of gold, while its extinction coefficient is much lower. Both materials will be referred to as metals. The conducting walls are coated with a thin layer of SiO_2 (see Fig. 1). The structure is filled with a fluid, such as water, instead of air, for the purpose of application as a biosensor.

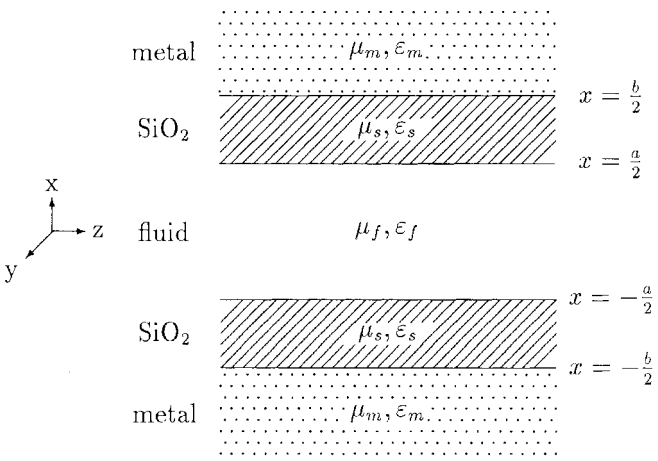

Fig. 1. Symmetric five-layer waveguide structure.

It is a well-known property of a loss-free asymmetric three-layer slab waveguide (see Fig. 2) that waves become confined to the middle region which is surrounded by two media, infinitely extended in the x-direction, when its thickness reaches a certain value. Such a critical thickness is determined by the relative refractive indices of the three media and the wavelength, and is usually called the cutoff thickness for wave propagation in the structure [6]. In the five-layer waveguide of interest in this study (Fig. 1) the distance between the metal plates must be larger than the cutoff value for the used wavelength to allow wave propagation in the structure. Adding the coatings does not dramatically change the propagation characteristics as long as their thicknesses are small. The wave will propagate mainly in the fluid. However, once the thicknesses of the coatings exceed a certain value it is to be expected that the wave will propagate in the coating as well, with a potentially significant effect on the overall wave attenuation and phase constant. This thickness of the coatings is called the cutoff thickness, since it is associated with the onset of wave propagation in the coating and the significant reduction of propagation in the fluid [7].

Manuscript received December 1, 1995; revised November 21, 1996. The work of W. E. A. Van Petegem was supported by the Flemish and Canadian (Alberta) governments.

W. Van Petegem was with the Department of Electrical Engineering, University of Alberta, Edmonton, Alta., Canada T6G 2G7. He is now with the Department of Biomechanics, Katholieke Universiteit Leuven, B-3001 Heverlee, Belgium.

C. R. James, F. E. Vermeulen, and A. M. Robinson are with the Department of Electrical Engineering, University of Alberta, Edmonton, Alta., Canada T6G 2G7.

Publisher Item Identifier S 0018-9480(97)01729-8.

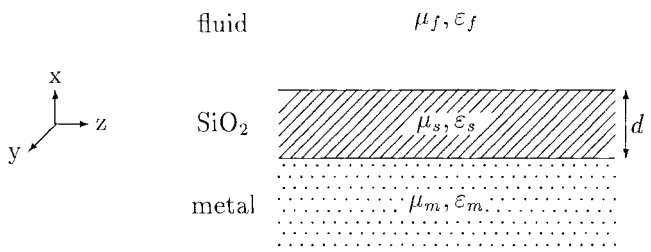

Fig. 2. Asymmetric three-layer slab waveguide structure.

TABLE I
COMPLEX REFRACTIVE INDICES FOR WAVEGUIDE MATERIALS AT $\lambda = 1\,\mu$M

material	n	k
Au	0.257	6.820
Si	3.592	0.006
SiO_2	1.450	0.0002
H_2O	1.321	0.000003

This paper begins with a theoretical analysis of a parallel planar waveguide with thin coatings. In the analysis, the characteristic equations for the different modes are derived. Following this, numerical results are presented for the attenuation and phase constant of the lowest order modes, as a function of the coating layer thickness. These results reveal, for some modes and materials, a sudden transition in the propagation path from the fluid to the coating. It is suggested how this property may be exploited for biosensor applications, such as an optical immunosensor, where detection is based on a change in coating thickness due to the binding of immunocomponents at the waveguide surface.

II. THEORETICAL ANALYSIS

A. Model Description

Consider the five-layer waveguide structure shown in Fig. 1. This structure is an idealization of a waveguide that consists of a fluid between two parallel metal plates, each of finite thickness and coated with a thin layer of SiO_2. Each layer is characterized by its magnetic permeability (μ) and its complex electric permittivity (ε). Subscripts identify the various layers ($f \equiv$ fluid, $s \equiv SiO_2$, and $m \equiv$ metal).

The complex refractive index N of a medium is defined by

$$N = n - jk \tag{1}$$

where n is the refraction index of the medium and k its extinction coefficient. Values for the complex refractive index at a wavelength of $1\,\mu$m for the materials to be considered here are summarized in Table I [8], [9]. Note that [9] does not explicitly mention a value for the extinction coefficient of Si at $1\,\mu$m. The value stated in Table I is approximate. It is inferred from equations in [9] and, in fact, this approximation does not critically affect the results presented here.

B. Characteristic Equations

The approach taken here to treat electromagnetic (EM) wave propagation in the guiding structure of Fig. 1 is similar to that in [1] and [6].

The propagation constant γ of a wave in the guide is defined as

$$\gamma = \alpha + j\beta \tag{2}$$

where α denotes the attenuation constant and β the phase constant.

Since the structure of Fig. 1 is uniform along the z-axis and infinite in the y-direction, Maxwell's equations yield the following propagating modes:

- TE modes, with field components: E_y, H_x ($\propto E_y$), and H_z ($\propto \partial E_y/\partial x$);
- TM modes, with field components: H_y, E_x ($\propto H_y$), and E_z ($\propto \partial H_y/\partial x$).

The mathematical derivation of the characteristic equations for both modes is straightforward.

1) TE Modes: Consider the TE modes first.

For notational convenience, the following parameters are introduced:

$$K_f^2 = \gamma^2 + \omega^2\mu_f\varepsilon_f \tag{3}$$

$$K_s^2 = \gamma^2 + \omega^2\mu_s\varepsilon_s \tag{4}$$

$$K_m^2 = \gamma^2 + \omega^2\mu_m\varepsilon_m \tag{5}$$

where ω is the radian frequency.

Since the field intensities have to vanish at infinity, the authors choose the solution (for $x > 0$):

$$E_{ym}(x) \propto e^{-jK_m x} \tag{6}$$

assuming that:

$$\mathrm{Re}\,(+jK_m x) > 0. \tag{7}$$

Continuity conditions are then imposed on the tangential field components E_y and H_z at the two interfaces $|x| = a/2$ and $|x| = b/2$. It can easily be shown that under these constraints only even or odd solutions are possible for $E_{yf}(x)$. Consequently, guided TE modes are divided into even and odd ones depending on the parity of E_y in the fluid layer. For each of both classes the characteristic equation can further be found by assuring the existence of matched EM-field intensities at the interfaces.

In the case of nonmagnetic materials ($\mu_s = \mu_f = \mu_m = \mu_0$, the magnetic permeability of free space), the characteristic equation for even TE modes is given by

$$\tan K_f\frac{a}{2} = j\frac{K_m}{K_f}\cdot\frac{1 + j\,\dfrac{K_s}{K_m}\tan K_s\dfrac{b-a}{2}}{1 + j\,\dfrac{K_m}{K_s}\tan K_s\dfrac{b-a}{2}} \tag{8}$$

and for odd TE modes

$$\tan K_f\frac{a}{2} = j\frac{K_f}{K_m}\cdot\frac{1 + j\,\dfrac{K_m}{K_s}\tan K_s\dfrac{b-a}{2}}{1 + j\,\dfrac{K_s}{K_m}\tan K_s\dfrac{b-a}{2}}. \tag{9}$$

Each solution of (8) and (9) determines the attenuation and the phase constant of an even mode and an odd mode, respectively. Numbering the consecutive solutions indicates the order of the mode.

It must be pointed out that the characteristic equation (8) and (9) can also be expressed by one equation, as is shown in [6] and [10].

2) TM Modes: A similar approach can be followed to find the characteristic equations for even TM modes:

$$\tan K_f \frac{a}{2} = j \frac{\varepsilon_f}{K_f} \cdot \frac{K_m}{\varepsilon_m} \cdot \frac{1 + j \frac{\varepsilon_m}{K_m} \cdot \frac{K_s}{\varepsilon_s} \cdot \tan K_s \frac{b-a}{2}}{1 + j \frac{\varepsilon_s}{K_s} \cdot \frac{K_m}{\varepsilon_m} \cdot \tan K_s \frac{b-a}{2}} \quad (10)$$

and for odd TM modes:

$$\tan K_f \frac{a}{2} = j \frac{\varepsilon_m}{K_m} \cdot \frac{K_f}{\varepsilon_f} \cdot \frac{1 + j \frac{\varepsilon_s}{K_s} \cdot \frac{K_m}{\varepsilon_m} \cdot \tan K_s \frac{b-a}{2}}{1 + j \frac{\varepsilon_m}{K_m} \cdot \frac{K_s}{\varepsilon_s} \cdot \tan K_s \frac{b-a}{2}}. \quad (11)$$

Again, consecutive solutions of these equations yield the propagation characteristics of all even and odd modes, respectively.

Without the SiO_2 coating on the metal walls of the structure of Fig. 1, the above characteristic equations for TE and TM modes can be simplified and are in agreement with the ones given in [1].

3) Three-Layer Slab Waveguide: A special case emerges when the distance between the metal plates increases without limit, but the coating thickness is kept constant ($a, b \to \infty$, but $(b-a)/2 = d$). This situation corresponds to the three-layer slab waveguide of Fig. 2. The left-hand side (LHS) of (9) and (10) reduces to

$$\lim_{a \to \infty} \tan K_f \frac{a}{2} = j \cdot \text{sign}\,[\text{Im}(K_f)] = -j \quad (12)$$

since only exponentially decaying field intensities are physically acceptable in infinite media. The characteristic equations now become

$$\tan K_s d = j \cdot \frac{K_s \cdot (K_m + K_f)}{K_s^2 + K_f \cdot K_m} \quad (13)$$

and

$$\tan K_s d = j \cdot \frac{\frac{K_s}{\varepsilon_s} \cdot \left(\frac{K_f}{\varepsilon_f} + \frac{K_m}{\varepsilon_m} \right)}{\frac{K_s^2}{\varepsilon_s^2} + \frac{K_m}{\varepsilon_m} \cdot \frac{K_f}{\varepsilon_f}} \quad (14)$$

for TE and TM modes, respectively. Note that the distinction between even and odd modes no longer exists for the structure of Fig. 2; equations (8) and (9) both reduce to (13), while (10) and (11) reduce to (14). These equations will be used later to calculate the coating cutoff thickness, at which propagation becomes possible in the SiO_2 layer.

C. Analytical Approximations

1) Propagation Constants: Initial estimates for γ are required when numerically solving the determinantal equations. For the lowest order TE and TM modes in a planar waveguide without a coating and filled with air, suitable approximations for γ are given in [1]. In the present study, propagation characteristics are analyzed as a function of the coating thickness. For zero thickness, the estimate in [1] applies and can be used to calculate the exact propagation constant. This result in turn serves as a starting value which guides the search for further roots of the characteristic equations as the layer thickness is incrementally increased.

2) Onset of Transition in Propagation Pathway from Fluid to Coating: A change in wave-propagation characteristics is expected as the coating thickness exceeds that value where cutoff occurs [7], [11]–[12]. Indeed, when the coating thickness is above its cutoff value a major part of the wave will propagate in the coating and not in the fluid.

The cutoff thickness of the coating, and hence the occurrence of the shift in propagation from one medium to another, can be predicted by a phase-matching condition [7], [11]–[12]; the phase shift of the propagating wave (expected to be predominantly in the coating when its thickness is larger than the cutoff thickness) should be approximately equal to the wavenumber in the fluid, the medium where the wave propagates before the cutoff in the coating occurs. In mathematical terms, this condition is

$$\beta \approx \frac{2\pi}{\lambda} n_f \quad (15)$$

when the extinction coefficient of the fluid (k_f) is neglected. At cutoff, the attenuation constant is generally very small ($\alpha \ll \beta$), and for simplicity of the calculations, it is ignored [7]; i.e.,

$$\alpha \approx 0. \quad (16)$$

Thus, the transition occurs when $K_f \approx 0$.

At the transition, the characteristic equations for TE modes become

$$\tan K_s d \approx j \frac{K_m}{K_s}. \quad (17)$$

Using the definitions of K_s and K_m and the optical properties given in Table I, it can be shown that for both wall materials (Au and Si)

$$K_s d \approx \frac{\pi}{2}. \quad (18)$$

Using (4), an approximation for the cutoff thickness of the coating can be obtained as

$$\frac{d}{\lambda} \approx \frac{1}{4\sqrt{n_s^2 - n_f^2}}. \quad (19)$$

From (19) and with the material properties mentioned in Table I, it follows that when the coating increases to a thickness of 0.42λ, the TE wave is no longer confined in the fluid (water), but starts propagating in the SiO_2 coating, whatever metal (Au or Si) is used. Similar behavior does not occur for TM modes.

This is not unexpected, since lack of a well-defined cutoff is a characteristic usually associated with a TM mode [11].

III. Simulation Results

In order to find the roots of the characteristic equations for each mode a numerical root solver based on Muller's method was implemented in MATLAB [14]. Results are presented here for the lowest order even and odd TE and TM modes. The wavelength λ in the simulations is chosen to be $1\,\mu$m.

A. TE Modes

The propagation constants for the lowest order even and odd TE modes are calculated from (8) and (9). The results are presented in Fig. 3, as a function of the coating thickness, with the metal spacing b as a parameter.

The attenuation constant α decreases with increasing metal spacing b. This behavior is well-expected [1]. Results for metal spacings b larger than $5\,\mu$m have been calculated as well, but are not shown. These results were found to be almost identical to the ones shown for $b = 5\,\mu$m, for both the attenuation and phase constant. Thus, increasing the metal spacing has little effect on the propagation constant once a value of about $5\,\mu$m is reached. Larger spacings will allow higher order modes to propagate, a situation which is generally undesirable for most applications.

Of significance is the shape of the attenuation constant curve for $b = 5\,\mu$m. For the smallest coating thicknesses (in the range from 0 to $0.3\,\mu$m), the attenuation constant is only slightly dependent on coating thickness. Increasing the coating thickness beyond this range causes a sudden increase of about one order of magnitude in the attenuation constant. The coating thickness at which this happens is about $0.4\,\mu$m, the value calculated above for the cutoff thickness. Beyond this thickness, the TE mode shifts from propagating in the fluid to propagating in the SiO_2 layer.

This latter statement is supported by the time-averaged power-flow distributions shown in Fig. 4. In this figure, the time-averaged power flow distribution is plotted against the distance x from the center of the waveguide. Symmetric profiles apply for the other half of the guide. The spacing b between the metal planes is chosen to be $5\,\mu$m, since a sharp transition in wave propagation from fluid to coating occurs at this value.

The power flow distribution is calculated by use of the Poynting vector

$$\langle \mathbf{S} \rangle = \tfrac{1}{2}\mathrm{Re}\,(\mathbf{E} \times \mathbf{H}^*) \tag{20}$$

and is normalized to equal $1W$ per-unit width in the y-direction. For both the even and odd TE modes, it can clearly be seen that the wave propagates mainly in the fluid when the thickness of the SiO_2 coating is less than the cutoff thickness. However, for a thickness of $0.5\,\mu$m, power flow has predominantly shifted from the fluid to the coating.

This transition in propagation path may also be demonstrated by comparing the wave propagation characteristics for the five-layer structure of Fig. 1 with those for the three-layer structure of Fig. 2. The propagation characteristics for the latter are calculated from (13). As can be seen in Fig. 3, the attenuation and phase constants become identical for both structures when $b = 5\,\mu$m, once the SiO_2 layer has been increased in thickness beyond its cutoff value for the lowest order TE mode. In fact, increasing the metal spacing in Fig. 1 is essentially equivalent to removing the upper boundary of the waveguide, to create a structure that resembles the one in Fig. 2. Hence, very similar wave propagation characteristics are expected. This can easily be verified in the case of $b = 5\,\mu$m, although not for $b = 2\,\mu$m.

There is also a difference in the attenuation and phase constants of the even and odd TE modes, when the wave is propagating in the fluid. Once the SiO_2 layer has been

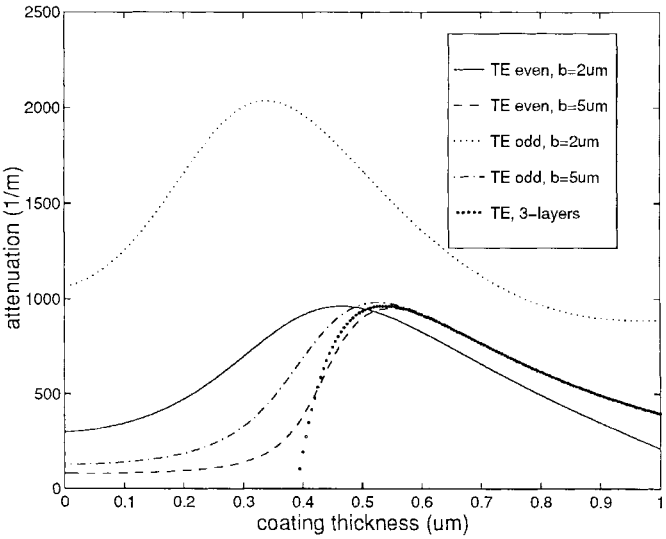

(a)

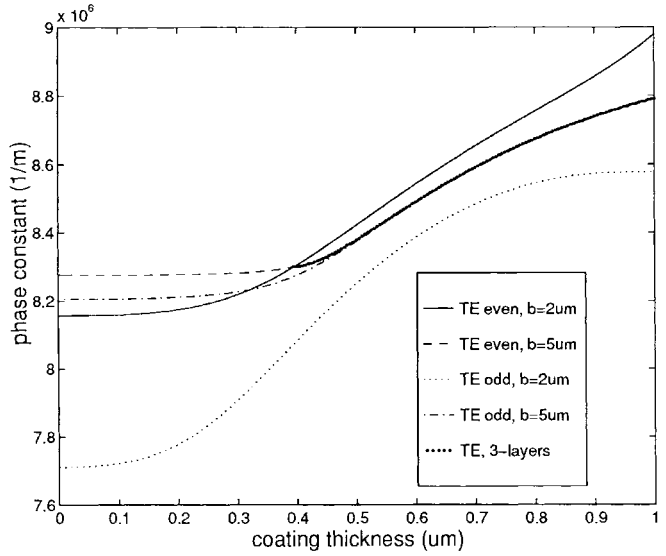

(b)

Fig. 3. (a) Attenuation and (b) phase constant of a wave in a five-layer waveguide with Au as the metal, SiO_2 as the coating, and water as the fluid plotted as a function of the coating thickness for the lowest order even and odd TE modes and metal spacings of $b = 2$ and $5\,\mu$m, and compared to the lowest order TE mode propagation characteristics in a three-layer waveguide of the same materials; note that the latter completely coincides with the odd TE mode in the five-layer structure.

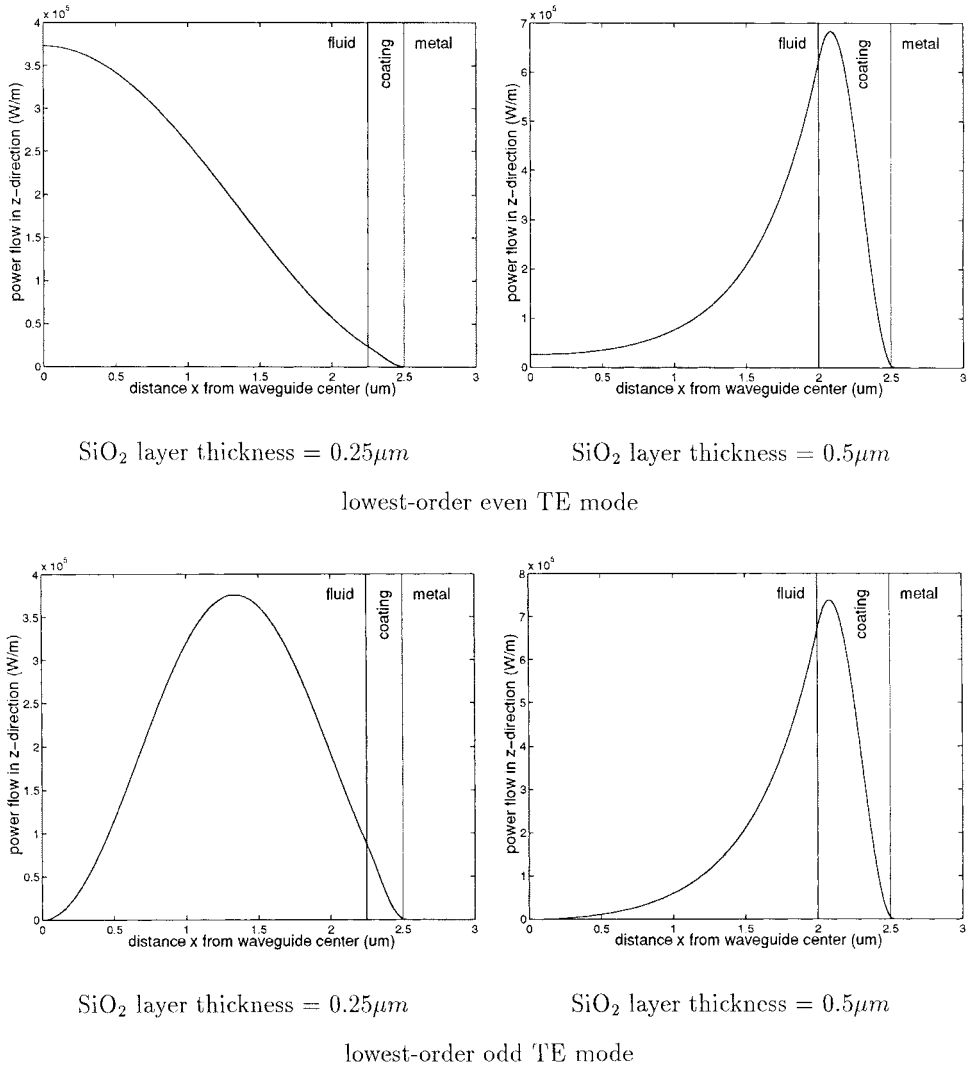

Fig. 4. Time-average power flow distributions normalized to $1W$ per-unit width in the y-direction, in the transverse plane of a five-layer waveguide with Au as the metal, SiO_2 as the coating, and water as the fluid plotted as a function of the distance x from the center of the structure for the lowest order even and odd TE modes and a metal spacing of $b = 5\,\mu$m.

increased beyond its cutoff thickness, these differences disappear. This is a further indication of the transition to a behavior typical of the waveguide structure of Fig. 2. Indeed, as previously mentioned, no distinction is possible between even and odd modes for such a slab waveguide.

A comparison between Au and Si as metal is made in Fig. 5 for a metal spacing $b = 5\,\mu$m. Both metals lead to a similar variation in wave propagation behavior for the lowest order TE modes as the coating thickness is varied although these metals have quite different optical properties. The phase shift is almost identical in both cases. The attenuation constant, however, is about an order of magnitude larger for Si than for Au. The cutoff thickness of the SiO_2 coating is approximately $0.4\,\mu$m, for both metals. This is in agreement with the theoretical analysis; equation (19) indeed shows that the cutoff thickness is not dependent on the properties of the metal. Although the attenuation constant is larger for Si than for Au, wave propagation for the Si exhibits a sharper transition from propagation in the fluid to propagation in the SiO_2 layer. This larger sensitivity (change in attenuation constant with change in coating thickness) makes Si potentially a more attractive material for microsensor applications, as discussed later.

B. TM Modes

As already indicated, the TM modes do not show the same transition in the propagation pathway as the TE modes when the thickness of the SiO_2 layer is increased.

The propagation constants of the even and odd lowest order TM modes are calculated from (11) and (10). The results are presented in Fig. 6, for a metal spacing $b = 5\,\mu$m and for both Au and Si as metal. In the case of Au, the attenuation and phase constants of the even and odd modes virtually coincide, for all SiO_2 coating thicknesses considered. The general shape of the attenuation and the phase constant curves remotely resembles the shape of the corresponding curves for TE modes in the case of Au, when this TE mode propagates in the SiO_2 layer (i.e., coating thickness above its cutoff value). This suggests that the TM modes are never propagated in the fluid, but always in the SiO_2 layer. Indeed, the power flow distributions shown in Fig. 7 show this to be the case. It should also be noted that

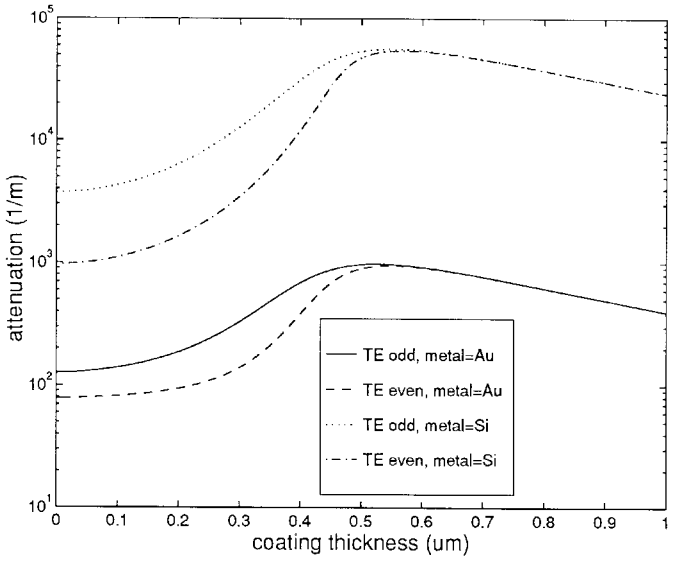

(a)

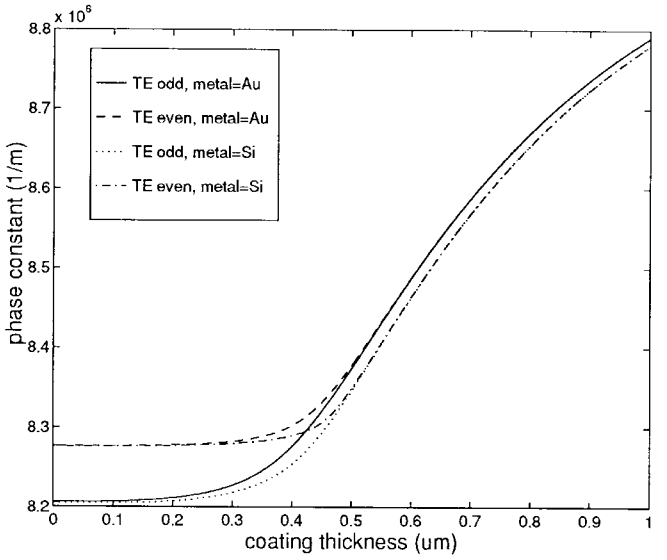

(b)

Fig. 5. (a) Attenuation and (b) phase constant of a wave in a five-layer waveguide with Au or Si as the metal, SiO_2 as the coating, and water as the fluid plotted as a function of the coating thickness for the lowest order even and odd TE modes and a metal spacing of $b = 5\,\mu$m.

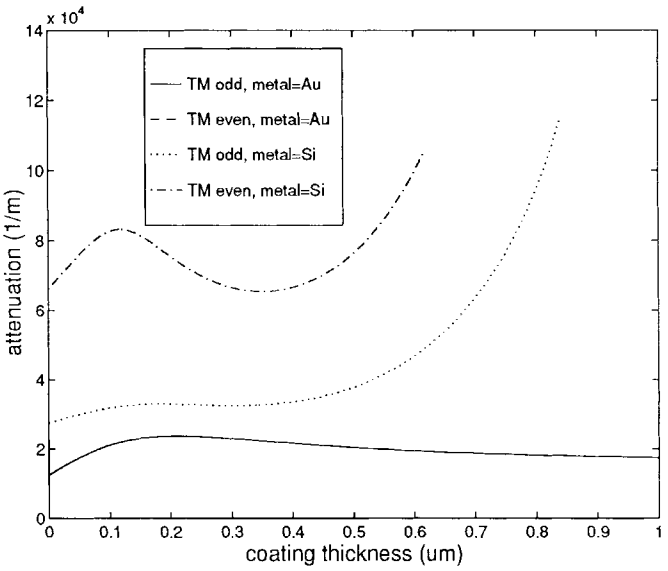

(a)

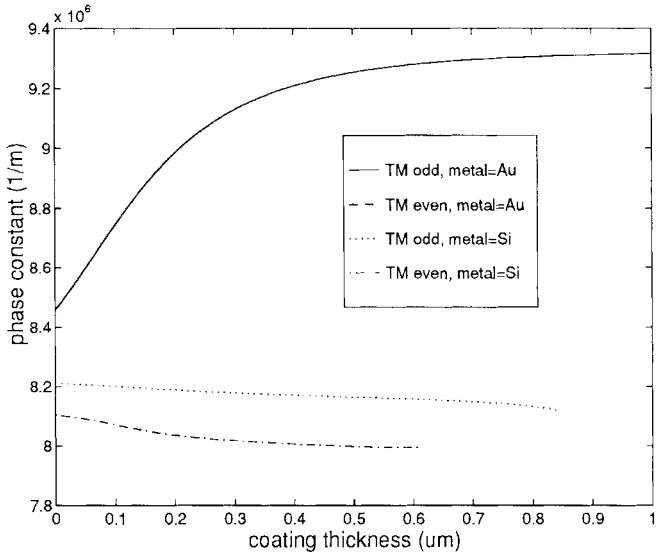

(b)

Fig. 6. (a) Attenuation and (b) phase constant of a wave in a five-layer waveguide with Au or Si as the metal, SiO_2 as the coating, and water as the fluid plotted as a function of the coating thickness for the lowest order even and odd TM modes and a metal spacing of $b = 5\,\mu$m; the curves for Si become discontinuous at a coating thickness for which solutions with a field intensity that decays exponentially in the Si can no longer be found; the curves for even and odd TM modes in the case of Au completely coincide in these plots.

the attenuation constant for TM modes is at least one order of magnitude larger than for TE modes.

When Si is used as a metal, the attenuation constant is higher than when Au is used (see Fig. 6). Moreover, the attenuation and phase constant curves become discontinuous at a certain coating thickness. For this thickness (and larger ones), no solutions can be found for (10) and (11), for which the field intensity decays exponentially in the metal. In all previous cases considered the field intensity in the metal decays very rapidly in the x-direction and hence the five-layer model of Fig. 1 is adequate for representing a structure having metal walls of finite thickness. In the present case, however, where the field intensity in the metal does not decay exponentially, the model of Fig. 1 is inappropriate for a structure with finite metal boundaries. A more detailed model is required to fully investigate the propagation characteristics for TM modes (as described in [10]) when Si is used as a metal.

IV. Sensor Applications of a Parallel Planar Waveguide Coated with a Thin Layer

A. Sensing Principle

Based on their propagation characteristics, TE modes show potential for use in sensing applications. TM modes are not

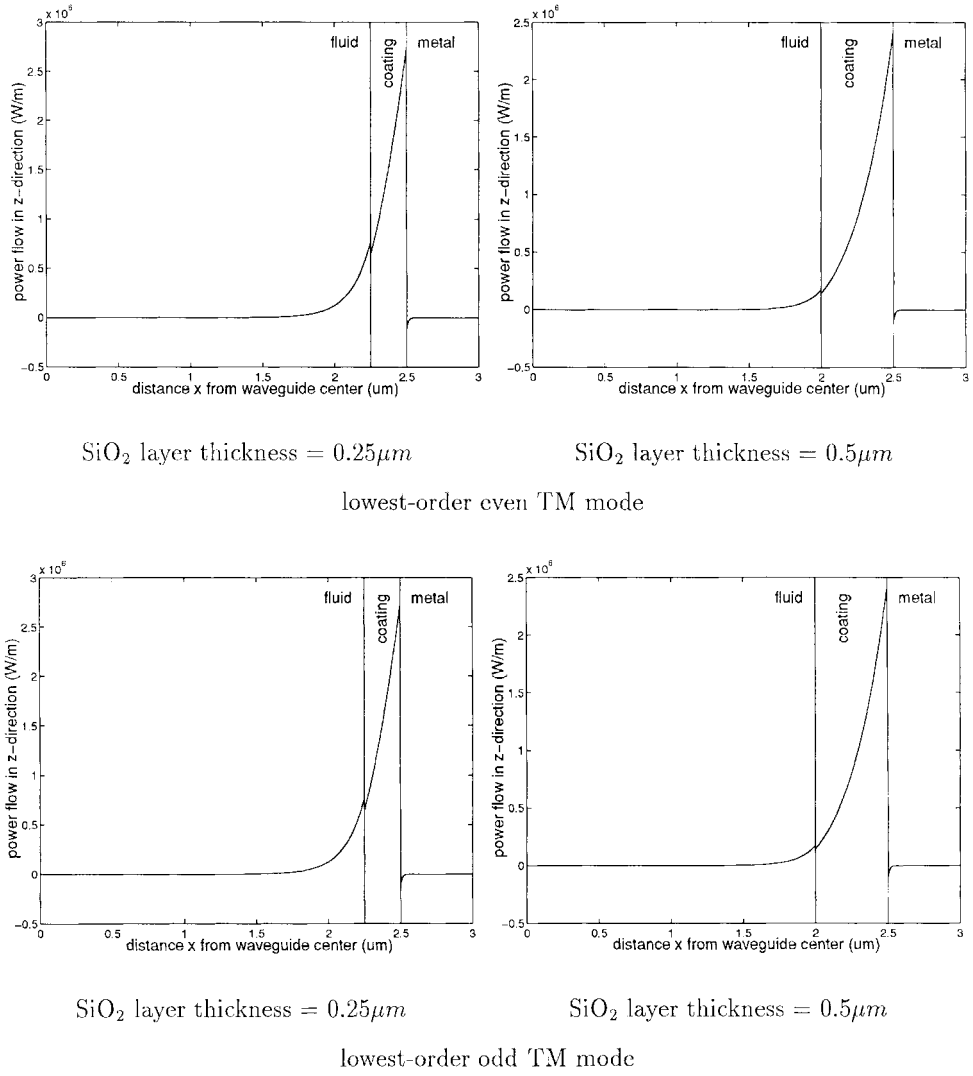

Fig. 7. Time-average power flow distributions normalized to $1W$ per-unit width in the y-direction, in the transverse plane of a five-layer waveguide with Au as the metal, SiO_2 as the coating, and water as the fluid plotted as a function of the distance x from the center of the structure for the lowest order even and odd TM modes and a metal spacing of $b = 5\,\mu$m.

suitable since they do not exhibit the transition in propagation pathway from fluid to SiO_2 layer. Therefore, the following discussion is limited to TE modes.

The transition in the propagation pathway is accompanied by a sudden increase in attenuation, a property that can be used in sensor applications. A relatively small change in the SiO_2 layer thickness will lead to a very large change in attenuation of the propagated wave. This occurs when the layer thickness increases from below to above the cutoff value. As shown in Fig. 5, the highest sensitivity occurs for odd TE modes. Comparing both wall materials considered, Si is more promising than Au. Although the attenuation constant reaches higher values for Si than for Au, thus reducing the overall propagation distance, the sudden increase in the attenuation constant with increase in coating thickness is much steeper for Si than for Au. Combined with the fact that it is relatively easy to grow a thin SiO_2 film on Si, this creates a favorable situation for practical implementations.

A common way to present the attenuation constant is to determine the number of wavelengths a wave propagates in the waveguide before its field intensity is reduced to $1/e$ of its original value. The authors then define sensitivity as the change in that propagated number of wavelengths per-unit change in SiO_2 layer thickness. The attenuation constant was calculated for fluid refractive indices in the range between 1.3 to 1.4, covering most physiological fluids [9], [15]. For each index, maximum sensitivity was determined and plotted in Fig. 8 for odd TE modes, for a structure with Si as metal and $b = 5\,\mu$m.

Fig. 8 shows that for the odd TE mode the maximum sensitivity for a fluid refractive index n_f of 1.3 is 55 λ/nm. For a given coating thickness, a $1\,\mu$m wave will propagate a certain number of wavelengths in the structure. An increase in thickness of the SiO_2 layer of 1 nm will reduce that number by 55 wavelengths (or $55\,\mu$m). Note that this is maximum sensitivity, which occurs when the initial coating thickness is chosen where the attenuation curve (Fig. 5) has its steepest slope, i.e., about $0.45\,\mu$m.

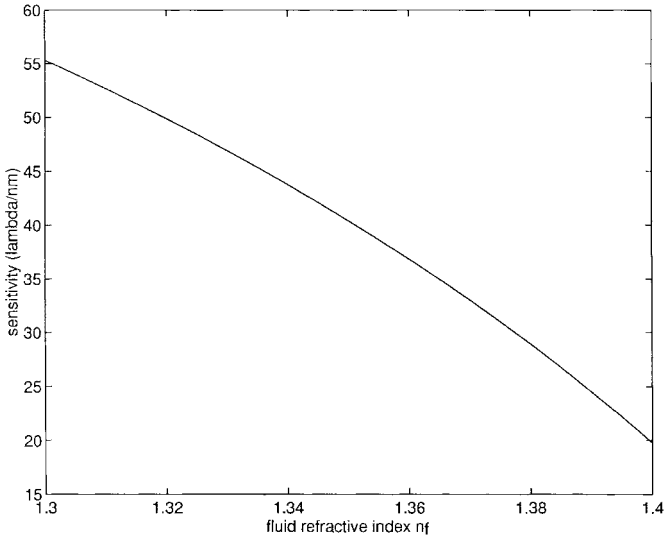

Fig. 8. Maximum sensitivity (i.e., change in number of wavelengths a wave is propagated before its intensity is reduced to $1/e$ of its original value, per-unit change in coating thickness) in a five-layer waveguide with Si as the metal, and SiO_2 as the coating, plotted as a function of fluid refractive index, for the lowest order even TE mode, and a metal spacing of $b = 5\ \mu$m.

For a range of the refractive index n_f between 1.3–1.4, the maximum sensitivity varies from 55 to 20 λ/nm. This should be in all cases experimentally detectable.

B. Application

The steep increase in attenuation constant and its high sensitivity with respect to an increase in coating layer thickness has potential value for biosensor applications. One such application is an optical immunosensor [16].

Indeed, a micromachined Si waveguide can be coated with a SiO_2 layer, up to a thickness of about $0.45\ \mu$m, where maximum sensitivity occurs as indicated in Fig. 5. A layer of (capture) antibodies is then bound to that surface. A TE mode will propagate over a certain distance in the coated waveguide. Whenever a physiological test fluid containing the specific antigens is flowing through the fluid region of the structure, these antigens will bind to their respective antibodies, hereby increasing the thickness of the coating layer by a few tens of nm. As a result, it immediately decreases the propagation distance for a 1-μm wave by at least $100\ \mu$m (see Fig. 8), since the operation region is chosen to have maximum sensitivity. Measuring such a change in propagation distance can be realized with state-of-the-art integrated optics.

Several problems can be expected in the practical development of this type of immunosensor: the binding procedure for the immunocomponents, the flow of physiological fluid through microchannels, the minimum detectable amount of antigens, and the appropriate calibration procedure. These practical problems, however, have been solved before for other applications (see, e.g., [17]–[19]).

V. Conclusion

In this paper, the influence of an SiO_2 layer coating a planar waveguide structure filled with a fluid is analyzed both analytically and numerically. The characteristic equations for the even and odd TE and TM modes are derived. Roots of these equations are calculated numerically and yield the respective attenuation and phase constants. From these results it becomes clear that the lowest order TE modes are propagated in the fluid for very thin SiO_2 coatings. As the SiO_2 coating thickness exceeds its cutoff value the mode is propagated in the coating and no longer in the fluid. A possible application of this transition in the propagation pathway is its use as a detection principle for an optical immunosensor. The lowest order TM modes do not show this behavior for the materials considered.

Acknowledgment

The authors wish to thank Dr. T. Mosmann, Dr. L. Phlak, and Dr. L. Guilbert, all at the Department of Immunology, University of Alberta, Edmonton, AB, Canada, for many practical discussions on the development of an optical immunosensor. The stimulating and inspiring thoughts of their colleague, Dr. T. Wegmann, who unfortunately passed away while this work was going on, are especially remembered and acknowledged.

References

[1] F. E. Vermeulen, C. R. James, and A. M. Robinson, "Hollow microstructural waveguides for propagation of infrared radiation," *J. Lightwave Tech.*, vol. 9, no. 9, pp. 1053–1060, Sept. 1991.

[2] F. E. Vermeulen, T. Wang, C. R. James, and A. M. Robinson, "On the propagation of infrared radiation in hollow microstructural cylindrical waveguides," *J. Lightwave Tech.*, vol. 11, no. 12, pp. 1956–1964, Dec. 1993.

[3] F. E. Vermeulen, A. M. Robinson, C. R. James, and J. N. McMullin, "Infrared surface waves in circular hollow waveguides with small core diameters," *IEEE Trans. Microwave Theory Tech.*, vol. 42, pp. 1932–1938, Oct. 1994.

[4] Y. Kato and M. Miyagi, "Modes and attenuation constants in circular hollow waveguides with small core diameters for the infrared," *IEEE Trans. Microwave Theory Tech.*, vol. 40, pp. 679–685, Apr. 1992.

[5] ——, "Numerical analysis of mode structures and attenuations in dielectric-coated circular hollow waveguides for the infrared," *IEEE Trans. Microwave Theory Tech.*, vol. 42, pp. 2336–2342, Dec. 1994.

[6] P. Yeh, *Optical Waves in Layered Media.* New York: Wiley, 1988, ch. 11, pp. 298–374.

[7] M. Marciniak, J. Grzegorzewski, and M. Szustakowski, "Analysis of lossy mode cut-off conditions in planar waveguides with semiconductor guiding layer," *Proc. Inst. Elect. Eng.*, vol. 140, pp. 247–252, Aug. 1993.

[8] E. D. Palik, Ed., *Handbook of Optical Constants of Solids.* Orlando, FL: Academic, 1985.

[9] ——, *Handbook of Optical Constants of Solids II.* Boston, MA: Academic, 1991.

[10] M. Miyagi and S. Nishida, "A proposal of low-loss leaky waveguide for submillimeter waves transmission," *IEEE Trans. Microwave Theory Tech.*, vol. MTT–28, pp. 398–403, Apr. 1980.

[11] T. E. Batchman and G. M. McWright, "Mode coupling between dielectric and semiconductor planar waveguides," *IEEE J. Quantum Electron*, vol. QE-18, pp. 782–788, Apr. 1982.

[12] G. M. McWright, T. E. Batchman, and M. S. Stanziano, "Measurement and analysis of periodic coupling in silicon-clad planar waveguides," *IEEE Trans. Microwave Theory Tech.*, vol. MTT-30, pp. 1753–1759, Oct. 1982.

[13] S. D. Conte, *Elementary Numerical Analysis, An Algorithmic Approach*, Information Processing and Computers. New York: McGraw-Hill, 1965.

[14] The Mathworks, Inc., *MATLAB 4.2 for UNIX Computers, User's Guide*, Natick, MA: MATLAB, 1994.

[15] R. Weast and M. Astle, Eds., *CRC Handbook of Chemistry and Physics.* Boca Raton, FL: CRC Press, 1981.

[16] W. Van Petegem, C. R. James, F. E. Vermeulen, and A. M. Robinson, "Numerical analysis of near-infrared wave propagation properties in a coated parallel planar waveguide structure for micromachined

immunosensor applications," presented at the 17th Ann. IEEE/EMBS Conf., Montréal, P.Q., Canada, Sept. 1995.
[17] A. P. F. Turner, I. Karube, and G. S. Wilson, Eds., *Biosensors, Fundamentals, and Applications.* London, U.K.: Oxford Univ. Press, 1987.
[18] R. F. Taylor, Ed., *Protein Immobilization: Fundamentals and Applications*, (Bioprocess technology series, no. 14). New York: M. Dekker, 1991.
[19] D. J. Harrison, K. Fluri, K. Seiler, Z. Fan, C. S. Effenhauser, and A. Manz, "Micromachining a miniaturized capillary electrophoresis-based chemical analysis system on a chip," *Science*, vol. 261, pp. 895–897, Aug. 1993.

Wim E. A. Van Petegem was born in Sint-Amandsberg, Belgium, in 1964. He received the M.Sc. degree in electrical engineering from the University of Ghent, Ghent, Belgium, in 1987, the M.Sc. degree in biomedical engineering from the University of Leuven, Heverlee, Belgium, in 1989, and the Ph.D. degree from the University of Leuven in 1993.

From October 1993 to September 1994, he did Post-Doctoral research on new developments for optical immunosensors at the University of Alberta, Edmonton, Alta., Canada. Since October 1994, he has been a Post-Doctoral Researcher at the University of Leuven, Division of Biomechanics and Engineering Design and his educational tasks are situated in the postgraduate program in Biomedical and Clinical Engineering at the same university. His present research interest is in rehabilitation engineering.

C. Robert James was born in Vancouver, B.C., Canada, in 1935. He received the B.A.Sc., M.Sc., and Ph.D. degrees in electrical engineering from the University of British Columbia, Vancouver, B.C., Canada, in 1960, 1961, and 1964, respectively. From 1964 to 1965 he was a NATO/NRC Post-Doctoral Fellow at Oxford University, Oxford, U.K., in Theoretical Physics.

Following his work at Oxford University, he assumed an appointment as an Assistant Professor of Electrical Engineering at the University of Alberta, Edmonton, Alta., Canada. In 1971, he became a full Professor and from 1974 to 1987 was Chairman of the Electrical Engineering Department, at which time he became Vice President (Research) at the University of Alberta. His research has been in the fields of laser-plasma interactions, electromagnetic theory, and microstructural devices.

Dr. James is a member of the American Physical Society, the Canadian Association of Physicists, and the Canadian Society of Electrical and Computer Engineering.

Fred E. Vermeulen (S'59–M'62) was born in Stuttgart, Germany. He received the B.Sc. degree from the University of Alberta, Edmonton, Alta, Canada, the M.A.Sc. degree from the University of British Columbia, Vancouver, B.C., Canada, and the Ph.D. degree from the University of Alberta in 1959, 1962, and 1966, respectively, all in electrical engineering. From 1966 to 1967, he was a National Research Council Post-Doctoral Fellow at the European Organization for Nuclear Research in Geneva, Switzerland, where he was engaged in the study of space charge problems as related to the transport of ion beams.

In 1967 he assumed an academic position at the University of Alberta where he is currently a Professor of Electrical Engineering. His research is in applied electromagnetics, a particular interest being the physical and numerical modeling of wave propagation and electromagnetic heating in lossy materials.

Alexander M. Robinson was born in Vancouver, B.C., Canada, in 1938. He received the B.A.Sc., M.Sc., and Ph.D. degrees in engineering physics and plasma physics from the University of British Columbia, Vancouver, B.C., in 1961, 1963, and 1966, respectively.

He spent the next five years at the Defence Research Board, Valcartier, Quebec, working on the development of atmospheric pressure CO_2 lasers. In 1971, he joined the Electrical Engineering Department at the University of Alberta, Edmonton, Alta., becoming a Full Professor in 1976. His research there has been on CO_2 lasers, molecular spectroscopy, solar energy heating, photovoltaic systems, and more recently micromachining and microsensors. From 1984 to 1990, he was Director of the Computer Engineering Program at the University of Alberta.

Dr. Robinson is a member of OSA, Canadian Association of Physicists, Solar Energy Society of Canada and the International Solar Energy Society.